This is a preprint, the final version is subject to change, of the American Mineralogist (MSA)
Cite as Authors (Year) Title. American Mineralogist, in press.
(DOI will not work until issue is live.) DOI: http://dx.doi.org/10.2138/am-2017-6127

An experimental approach to quantify the effect of tetrahedral boron in tourmaline on the boron isotope fractionation between tourmaline and fluid

Revision 1

Authors:

Martin Kutzschbach[1*], Bernd Wunder[2], Robert B. Trumbull[2], Alexander Rocholl[2], Anette Meixner[3], Wilhelm Heinrich[2]

[1]Fachgebiet Mineralogie-Petrologie, Technische Universität Berlin, 13355 Berlin, Germany

[2]GeoForschungsZentrum Potsdam, 14473 Potsdam, Germany

[3]Faculty of Geosciences & MARUM-Center for Marine Environmental Sciences, University of Bremen, 28359 Bremen, Germany

*E-mail: martin.kutzschbach@gmx.de

This is a preprint, the final version is subject to change, of the American Mineralogist (MSA)
Cite as Authors (Year) Title. American Mineralogist, in press.
(DOI will not work until issue is live.) DOI: http://dx.doi.org/10.2138/am-2017-6127

ABSTRACT

This study investigates the effect of tetrahedral B ($^{[4]}$B) in synthetic tourmaline on the B isotope fractionation between tourmaline and fluid. This is important for the correct interpretation of B-isotope variations in natural tourmalines containing "excess" B (greater than 3 atoms per formula unit), which substitutes for Si at tetrahedral sites. Such tourmalines commonly occur in Li, Al-rich pegmatites and have been reported from glaucophane schists that formed at high pressures during subduction.

Tourmaline synthesis experiments were performed in a piston-cylinder apparatus in the system SiO_2-Al_2O_3-B_2O_3-NaCl-H_2O at 4 GPa and 700°C using different run durations, starting from quartz-γ-Al_2O_3-H_3BO_3 solid mixtures and NaCl-solutions. We were able to produce "olenitic" tourmaline with excess B between 1.2 and 2.5 $^{[4]}$B per formula unit. The B isotope compositions of the olenitic tourmaline and coexisting fluids were determined by secondary ion mass spectrometry and multi-collector plasma source mass spectrometry to derive isotope fractionation coefficients. The results indicate that for every 10 mol % of total B in tourmaline in tetrahedral coordination, the value of $\Delta^{11}B_{tur\text{-}fluid}$ is shifted to more negative values by about 1 ‰ at 700°C. This is in good agreement with published *ab initio* calculations and corresponds to an intracrystalline fractionation of B-isotopes between the trigonal B and tetrahedral T sites of tourmaline on the order of 8 ± 5 ‰, whereby ^{10}B partitions to the T site.

INTRODUCTION

The use of boron isotope studies as an indicator of fluid source(s) and a tracer of fluid-rock interaction is well established. Depending on the mineralogical, chemical and isotopic composition of the B source, fluid-rock ratios, prevailing *P-T* and closed versus open system conditions, the B isotope ratios of natural fluids vary significantly (e.g., van Hinsberg et al. 2011). Because *in situ* sampling of (paleo) fluids is impossible in most cases, the isotopic composition must be determined indirectly through the analysis of hydrothermal minerals containing boron. Tourmaline is by far the most commonly used mineral for this purpose because it is stable over a wide range of *P-T* conditions (up to 7 GPa, 900°C, Krosse 1995), it occurs in a large variety of magmatic, metamorphic and sedimentary rocks and it is chemically and physically robust (e.g., Henry and Dutrow 1996).

The use of tourmaline as a fluid monitor requires knowledge about the equilibrium B isotope fractionation between tourmaline and fluid ($\Delta^{11}B_{tur\text{-}fluid}$). Experimental studies of tourmaline-fluid fractionation have so far addressed common tourmaline compositions where boron is exclusively in trigonal coordination (Meyer et al. 2008; Palmer et al. 1992). These results are applicable to most natural tourmalines but there are other cases where boron also occupies tetrahedral T-sites (*e.g.*, Ertl et al. 1997; 2005; 2006; 2007; Hughes et al. 2000; 2004; Kalt et al. 2001; Schreyer et al. 2002; Tagg et al. 1999). In those tourmalines, $^{[4]}B$ is incorporated in exchange for Si (Kutzschbach et al. 2016; Schreyer et al. 2000) and this seems to be favored in very Al-rich tourmaline with a large olenite component [$NaAl_3Al_6Si_6O_{18}(BO_3)_3O_3(OH)$] and at high pressures and low temperatures (Ertl et al. 2008). Examples are known from granitic pegmatites with up to 0.83 $^{[4]}B$ pfu (Ertl et al. 2008) and from blueschist facies glaucophane-schists with up to 0.26 $^{[4]}B$ pfu (Marschall et al. 2004).

77 The driving force for B-isotope fractionation is the bonding environment, with the light
78 ^{10}B isotope preferring the higher coordination number or more precisely longer bonds (Kowalski
79 et al. 2013, Kowalski and Wunder 2017, MacGregor et al. 2013). Thus it is expected that the
80 presence of tetrahedral boron in tourmaline will affect the tourmaline-fluid fractionation. The
81 magnitude of this effect was predicted by a*b initio* calculations (Kowalski et al. 2013), which
82 suggest that for every 10 mol% $^{[4]}B_{tot}$[1], the $\Delta^{11}B_{tur\text{-}fluid}$ value is shifted by 0.9 ‰ towards more
83 negative values (for olenitic compositions at 700°C). However, the effect has so far not been
84 experimentally studied, mainly due to the difficulty in synthesizing $^{[4]}B$-bearing tourmaline large
85 enough for *in situ* B isotope analysis. Kutzschbach et al. (2016; 2017) were able to produce
86 crystals up to 30 x100 μm of olenitic tourmaline containing up to 45 mol% $^{[4]}B_{tot}$. Based on these
87 materials, we set out to evaluate the isotopic effect of $^{[4]}B$ in tourmaline on isotopic fractionation
88 with aqueous fluid.
89
90 **SAMPLE MATERIAL AND ANALYTICAL METHODS**
91
92 **Tourmaline synthesis experiments**
93 Tourmaline analysed in this study was taken from Kutzschbach et al. (2016), who synthesized
94 $^{[4]}B$ bearing olenites in a piston cylinder apparatus at 4 GPa/700°C from a homogenous mixture
95 of quartz, γ-Al_2O_3, H_3BO_3 and a 5.4 mol/l NaCl solution. After 216 h run duration, tourmaline
96 occurs in two habits, i.e. columnar crystals (80 vol%) and slightly smaller radial acicular
97 aggregates (20 vol%). Besides their habit, the crystal populations are distinguishable by their
98 amount of $^{[4]}B$. Whereas the columnar crystals are homogenous and low in $^{[4]}B$ (29 mol% $^{[4]}B_{tot}$)
99 the acicular crystal are more B-rich and also zoned with respect to B content (cores: 45 mol%

[1] $^{[4]}B$ (mol%) = $^{[4]}B$ (pfu)/[$^{[4]}B$ (pfu)+ $^{[3]}B$ (pfu)]
pfu = atoms per formula unit

100 $^{[4]}B_{tot}$; rims: 32 mol% $^{[4]}B_{tot}$). Trace amounts of coesite and the hydroxyl-analogue of jeremejevite
101 [$Al_6(BO_3)_5(OH)_3$] have been detected with the latter forming inclusions in tourmaline. In the
102 following the hydroxyl-analogue of jeremejevite is simply referred to as jeremejevite.
103 By performing two experiments using the same initial bulk composition and *P-T* conditions but
104 shorter run durations of 0.5 and 2.5 h, Kutzschbach et al. (2017) noticed a distinct crystallization
105 sequence. Within the first 0.5 h, all of the solid γ-Al_2O_3 in the starting material reacts with the B-
106 rich starting fluid to form jeremejevite. The latter serves as a precursor for tourmaline
107 mineralization, which begins with the heterogeneous nucleation[2] of the acicular olenite crystals.
108 With increasing experimental run duration, jeremejevite successively dissolves and more olenite
109 forms, either by growth of the early acicular crystals or by later homogeneous nucleation[2] and
110 growth of the columnar crystals (Kutzschbach et al. 2017).
111 It has been noticed that jeremejevite preferentially fractionates ^{10}B, which leads to an
112 increase in $\delta^{11}B$ from -5.9(1) ‰ in the starting fluid to -3.2(2) ‰ in the fluid after 0.5 h
113 (Kutzschbach et al. 2017, Table 1). Due to the later dissolution of jeremejevite, the $\delta^{11}B$ of the
114 fluid decreases by about 2 ‰ from -3.2(2) ‰ in the fluid after 0.5 h to -5.2(2) ‰ in the fluid after
115 216 h (Kutzschbach et al. 2017, Table 1).
116
117 **Secondary ion mass spectrometry (SIMS)**
118 Boron isotope analyses were performed with the Cameca 1280-HR SIMS instrument at the GFZ-
119 Potsdam from flat and polished 1-inch epoxy mount of the samples. Prior to analysis, the samples
120 were cleaned with ethanol in an ultrasonic bath, then sputter coated in a vacuum with 35 nm of
121 high-purity gold. Results were obtained in two measurement sessions (S1: July, 2015 and S2:

[2] Heterogeneous nucleation is the formation of nucleation sites on surfaces whereas homogeneous nucleation occurs in the interior of a homogenous substance.

June, 2016). Differences in analytical parameters between the two sessions are indicated in square brackets. The analyses were done with a nominal 13 kV, 5 nA $^{16}O^-$ primary beam [S2: 3 nA], focused to a 5 μm [S2: 4 μm] spot on the sample surface (spot sizes were determined after measurement). Each analysis was preceded by a 90 s pre-burn on a 10 μm x 10 μm raster to remove the gold coating and establish stable sputtering conditions. Positive secondary ions were extracted using a +10 kV potential applied to the sample holder. A 400 μm diameter contrast aperture, a 3000 μm field aperture [S2: 4000μm] and a 50 V energy window were used without application of a voltage offset. The instrument was operated at a mass resolving power of $M/\Delta M \approx 2400$, which is sufficient to separate the $^{11}B^+$ from the $^{10}B^1H^+$ mass station ($\Delta M = 900$) and $^{10}B^+$ from the $^9Be^1H^+$ mass stations ($\Delta M = 1400$). Faraday cup multi-collection was applied for simultaneous measurement of ^{10}B and ^{11}B. The typical count rate for ^{11}B under these conditions was 1.61 x 10^7 ions per second for ^{11}B and 0.41 x 10^7 ions per second for ^{10}B [S2: 1.43 x 10^7 for ^{11}B and 0.36 x 10^7 for ^{10}B]. Each analysis comprised 20 mass scans (4 blocks of 5 measurements), resulting in a total analysis time of about 3 minutes.

Determination of instrumental mass fractionation (IMF) and monitor of analytical quality requires analysis of a matrix-matched reference material (RM). For tourmaline, we used the established RMs Harvard 112566 (schorl), Harvard 108796 (dravite) and Harvard 98114 (elbaite). Several authors noted a compositonal matrix effect in the SIMS analysis of B-isotopes in tourmaline (e.g. MacGregor et al. 2013; Chaussidon and Albarède 1992). This aspect was carefully considered in our study, particularly since the effect of tetrahedral B on the B isotope fractionation is expected to be subtle (Kowalski et al. 2013). Because none of the Harvard tourmaline RMs match the Fe- and Mg- free, Al-rich composition of the synthetic olenite (Fig. 1), we also prepared an in-house RM from a natural olenite crystal from a pegmatite near the Stoffhütte, Koralpe, Austria kindly provided by Andreas Ertl (Ertl et al. 1997). Electron

146 microprobe and SIMS verified homogeneity of both, major element and B isotope composition.
147 The $\delta^{11}B$ value of the olenite RM was determined independently by multi-collector plasma source
148 mass spectrometry (MC-ICP-MS). Details on the characterization of the olenite RM are presented
149 in the Appendix.

150 The internal precision of each analysis, expressed as the relative standard deviation from
151 the mean of 20 cycles is better than 0.4 ‰ (2 RSD_{mean}, Table 2). The repeatability, obtained from
152 multiple daily measurements of a particular RM (Table 2) was generally better than 1 ‰ (2
153 RSD). There is a significant difference of $^{11}B/^{10}B$ ratios for dravite between S1 and S2 (Table 2),
154 presumably due to different tuning, hence IMF correction was performed on a daily basis. In S2,
155 a systematic drift of the IMF values occurred over the measurement period of 5 hours, which was
156 accounted for using a linear regression based on multiple measurement of the olenite RM.
157 Multiple $^{11}B/^{10}B$ ratios were calculated according to the RMs used for IMF correction. After
158 correction for IMF, the $\delta^{11}B$ values were calculated relative to NIST SRM 951 using the $^{11}B/^{10}B$
159 ratio of 4.04362 from Catanzaro et al. (1970) and the relationship [$\delta^{11}B$ (‰) =
160 $\{[(^{11}B/^{10}B)_{sample}/(^{11}B/^{10}B)_{NIST\ SRM\ 951}] - 1\} * 1000$].
161

162 ## RESULTS
163

164 ### B isotope ratios of the synthetic tourmalines

165 Because the $\delta^{11}B$ value of the fluid changes as a function of experimental run duration (Table 1),
166 the B isotope ratios of olenite will also change and bulk analysis of tourmaline crystals is not an
167 appropriate method. Therefore, B isotope ratios of the synthetic tourmalines were analyzed using
168 SIMS. Three groups of crystals were analyzed (Fig. 2): columnar crystals (n = 4 in S1 and n=3 in
169 S2); columnar crystals with inclusions of jeremejevite (n = 3 in S1); and cores of the acicular
170 crystals (n = 6 in S2). All grains were measured in orientations perpendicular to the

crystallographic *c*-axis for reliable distinction between the crystal groups based on their habit. Imaging of the samples in BSE mode prior to SIMS analyses allowed for the detection of inclusion or cracks in the crystals (Fig. 2). For SIMS analyses only grains free of cracks were used. About half of the data points had to be rejected because of the small size of the crystals. For the same reason, no successful analysis of the acicular crystals rims was obtained.

By inspection of the $\delta^{11}B$ values using a particular RM, a relative shift of 0.8 ‰ towards more positive values is noted for the cores of the acicular crystals compared to the columnar crystals (Fig. 3, Table 3). In contrast, a shift of about 0.6 ‰ to more negative values (relative to the columnar crystals) is detected for the columnar crystals with jeremejevite inclusions. By performing an unpaired two-tailed t-test, the difference between the mean $\delta^{11}B$ of each crystal population is considered significant (p-value << 0.01). The same statistical test showed no significant change between the $\delta^{11}B$ values of columnar crystals obtained in the two sessions S1 and S2 (p-value ~0.53).

Depending on the RM, the absolute $\delta^{11}B$ values of a particular crystal population systematically deviate from each other (Fig. 3). Relative to the dravite RM, the mean $\delta^{11}B$ values are shifted by 2.7 ‰ and 3.3 ‰ towards more positive values using olenite or elbaite RMs, respectively (Table 3). For the schorl RM, a shift of 1.4 ‰ towards more negative values has been noticed relative to dravite.

DISCUSSION

Fractionation factor from Rayleigh fractionation modeling of fluids

Although experiments were performed with an excess of 300 mol% boron relative to the ideal olenite stoichiometry, the fluid shows a small but significant increase in $\delta^{11}B$ from -5.9(1) ‰ in

This is a preprint, the final version is subject to change, of the American Mineralogist (MSA)
Cite as Authors (Year) Title. American Mineralogist, in press.
(DOI will not work until issue is live.) DOI: http://dx.doi.org/10.2138/am-2017-6127

195 the starting fluid ($\delta^{11}B_{fluid\ ini}$) to -5.2(2) ‰ in the fluid after 216 h ($\delta^{11}B_{fluid\ fin}$); Table 1. Despite
196 the non-classical crystallization sequence with formation of jeremejevite (Kutzschbach et al.
197 2017), the net change of the fluid composition is interpreted to derive from closed system
198 crystallization of tourmaline only, as it is considered the only B bearing phase remaining in the
199 216 h experiment (neglecting trace amounts of jeremejevite inclusions preserved in tourmaline).
200 Following the procedure in Marschall et al. (2009), we are able to calculate an average $\Delta^{11}B_{tur\text{-}fluid}$
201 by knowing the $\delta^{11}B$ of the initial ($\delta^{11}B_{fluid\ ini}$) and final fluid ($\delta^{11}B_{fluid\ fin}$). Thus $\delta^{11}B_{fluid\ fin} = (1000$
202 $+ \delta^{11}B_{fluid\ ini}) \bullet F^{(1-\alpha)} - 1000$ and $\Delta^{11}B_{tur\text{-}fluid} = \delta^{11}B_{tur} - \delta^{11}B_{fluid} = 1000 \ln(\alpha^{-1})$, where F is the fraction
203 of B remaining in the fluid. Mass balance calculations show that no insoluble B-bearing quench
204 phases have formed in the 216 h experiment (Kutzschbach et al. 2017). Thus, for the 216 h
205 experiment $F = B_{fluid\ fin}$ (mg)/ $B_{fluid\ ini}$ (mg) = 0.69 mg/1.16 mg = 0.60 (Table 1). This results in a
206 fractionation factor $\alpha = 1.0014 \pm 0.0006$ and a $\Delta^{11}B_{tur\text{-}fluid} \approx -1.4 \pm 0.6$ ‰ (Fig. 4). The uncertainty
207 is estimated by propagating the uncertainty of $\delta^{11}B_{fluid\ ini}$ and $\delta^{11}B_{fluid\ fin}$, whereas the uncertainty
208 contribution of F is negligible. Based on the proportions of columnar crystals (80 vol%) and
209 acicular crystal (20 vol%) and their average composition, an average tetrahedral B content of 33
210 mol% $^{[4]}B_{tot}$ is estimated for the whole tourmaline fraction.
211 The result indicates that tourmaline fractionates the light ^{10}B. Thus, the fluid is expected
212 to become successively enriched in ^{11}B with experimental run duration and correspondingly, first
213 tourmalines should have more negative $\delta^{11}B$ values then tourmalines that form later. This is in
214 contrast to the results of the SIMS measurements, which show that the first tourmalines, i.e. the
215 cores of the acicular crystals, have $\delta^{11}B$ values about 0.8 ‰ higher compared to the columnar
216 crystals, which grow later (Table 3, Fig. 3). This inverse Rayleigh fractionation trend is due to the
217 decrease of $\delta^{11}B_{fluid}$ with experimental run duration (Table 1) and is related to the progressive
218 dissolution of metastable jeremejevite, which initially fractionates the ^{10}B. The affinity of

This is a preprint, the final version is subject to change, of the American Mineralogist (MSA)
Cite as Authors (Year) Title. American Mineralogist, in press.
(DOI will not work until issue is live.) DOI: http://dx.doi.org/10.2138/am-2017-6127

219 jeremejevite for ^{10}B is confirmed by the B isotope ratios obtained for columnar olenites with
220 jeremejevite inclusions as these are shifted by about 0.6‰ to more negative $\delta^{11}B$ compared to the
221 inclusion free columnar crystals (Fig. 3).
222
223 **Fractionation factor from combined SIMS and MC-ICP-MS analysis**
224 The fractionation coefficient calculated from the amount of Rayleigh fractionation only
225 represents an average value for the stable B isotope fractionation between bulk fluid and bulk
226 tourmaline. As the tourmalines are zoned with respect to $^{[4]}B$, the fractionation coefficient is
227 unlikely to be constant during the experiment. Based on the prediction of Kowalski et al. (2013),
228 a shift of the $\Delta^{11}B_{tur\text{-}fluid}$ to more negative values with increasing $^{[4]}B_{tot}$ is expected (Fig. 4). In
229 order to calculate how the $\Delta^{11}B_{tur\text{-}fluid}$ changes with the amount of $^{[4]}B$ in tourmaline in our
230 experiment, we need to know (i) the B isotope ratios of high and low $^{[4]}B$ tourmaline, i.e. the
231 cores of acicular crystals and the columnar crystals and (ii) the B isotope ratios of the fluids in
232 equilibrium with each of the two crystal populations.
233 As the acicular crystal grew first, it is reasonable to assume that the cores of the acicular
234 crystals were most likely in equilibrium with the fluid extracted from the 0.5 h experiments,
235 whereas the later columnar crystals were most likely in equilibrium with the fluid from the 216 h
236 experiment. Based on the $\delta^{11}B_{fluid}$ values measured by MC-ICP MS (Table 1) and the $\delta^{11}B_{tur}$ values
237 measured by SIMS (Table 3), $\Delta^{11}B_{tur\text{-}fluid}$ values are calculated with $\delta^{11}B_{tur} - \delta^{11}B_{fluid}$. Using the
238 olenite RM, which provides the best matrix match, $\Delta^{11}B_{tur\text{-}fluid} = -0.2 \pm 0.4$ ‰ for the columnar
239 crystals and -1.4 ± 0.4 ‰ for the cores of the acicular crystals (Table 4). This corresponds to a
240 relative shift of 1.2 ± 0.8 ‰ towards more negative $\Delta^{11}B_{tur\text{-}fluid}$ values for the cores of the acicular
241 crystals [45(3) mol% $^{[4]}B_{tot}$] compared to the columnar crystals [29(3) mol% $^{[4]}B_{tot}$]; Fig. 4. This
242 equals a shift of 0.8 ± 0.5 ‰ for each 10 mol% $^{[4]}B_{tot}$, which is used to calculate the

This is a preprint, the final version is subject to change, of the American Mineralogist (MSA)
Cite as Authors (Year) Title. American Mineralogist, in press.
(DOI will not work until issue is live.) DOI: http://dx.doi.org/10.2138/am-2017-6127

intracrystalline fractionation of B isotopes ($\Delta^{11}B_{[3]B_{tur}\text{-}[4]B_{tur}}$) using:

$$\Delta^{11}B_{[3]B_{tur}\text{-}[4]B_{tur}} = \Delta^{11}B_{[3]B_{tur}\text{-fluid}} - \Delta^{11}B_{[4]B_{tur}\text{-fluid}} \quad (1)$$

Given that 10 mol% $^{[4]}B_{tot}$ cause a shift of 0.8 ± 0.5 ‰ to more negative $\Delta^{11}B_{tur\text{-}fluid}$, additionally the following equations are valid:

$$\Delta^{11}B_{tur-fluid} = \Delta^{11}B_{[3]B_{tur}-fluid} \quad (2)$$

$$\Delta^{11}B_{tur-fluid} - 0.8 \pm 0.5‰ = 0.9 \cdot \Delta^{11}B_{[3]B_{tur}-fluid} + 0.1 \cdot \Delta^{11}B_{[4]B_{tur}-fluid} \quad (3)$$

By rearranging equations (2) and (3), it is calculated that $\Delta^{11}B_{[3]B_{tur}\text{-}[4]B_{tur}} = 8 \pm 5\ ‰$.

Comparison to *ab initio* calculations

The B isotope fractionation between $^{[4]}$B-free dravite and fluid from Meyer et al. (2008) is in agreement with the *ab initio* predictions of Kowalski et al. (2013; Fig. 4). Similarly, the results of the latter coincide with the fractionation factor obtained from Rayleigh fractionation modeling in our study (Fig. 4). Our SIMS data show a clear matrix effect in the comparison of IMF corrections using different tourmaline RMs (Fig. 3). Although we minimized this effect by using an in-house olenite RM, there might be a remnant bias due to matrix mismatch between the olenite RM and the synthetic olenite (Fig. 1). This might be a reason for the systematic offset of about 1 ‰ towards more positive $\Delta^{11}B_{tur\text{-}fluid}$ values (Fig. 4) compared to the predictions of Kowalski et al. (2013).

It might also stem from the fact that the fractionation coefficients of Kowalski et al. (2013) were calculated for a pressure of 0.1 MPa, whereas the synthesis experiments were performed at much higher pressure of 4.0 GPa. The high-pressure experiments yielded less extensive fractionation, which would be in agreement with results of Palmer et al. (1992), who

265 noticed less extensive B isotope fractionation at higher pressures within the pressure range of
266 0.05 – 0.2 GPa. In contrast, Meyer et al. (2008) did not observe an influence of pressure on
267 $\Delta^{11}B_{tur\text{-}fluid}$ between 0.2 and 0.5 GPa.

268 Another reason for the deviation between our fractionation data and the data of Kowalski
269 et al. (2013) might be presence of $(H_4BO_4)^-$ species in the experimental fluids. If 15 mol % of
270 additional $(H_4BO_4)^-$ species in the fluid are considered in the calculations of Kowalski et al.
271 (2013), the predicted $\Delta^{11}B_{tur\text{-}fluid}$ values are shifted by about 1 ‰ to more positive values, which
272 leads to a better agreement with our data (Fig. 4). However, for near neutral to acidic pH at which
273 the synthesis experiments have been performed, Schmidt et al. (2005) argued for negligible $^{[4]}B$
274 species in aqueous fluids at least in the pressure range 0.1MPa – 2 GPa.

275 Last but not least, small deviations might be caused by subtle differences in B-O bond
276 lengths. A single crystal X-Ray structure refinement of one of the columnar olenites from the 216
277 h experiment (Kutzschbach et al. 2016, their Table 4) reveals somewhat shorter $^{[3]}B$-O bond
278 lengths compared to the olenite used in the calculations of Kowalski et al. 2013 (1.365 Å vs.
279 1.378 Å). Since shorter B-O bonds increase the affinity for the heavy ^{11}B (Kowalski and Wunder
280 2017, MacGregor et al. 2013), one would expect higher $\Delta^{11}B_{tur\text{-}fluid}$ values in our study as
281 compared to the results of Kowalski et al. (2013), which matches our observations (Fig. 4).
282

283 **Influence of temperature on intracrystalline B isotope fractionation in tourmaline.**
284 The results of our study confirm the *ab initio* calculation of Kowalski et al. (2013) predicting that
285 tetrahedral B shifts the $\Delta^{11}B_{tur\text{-}fluid}$ to more negative values. This implies an intracrystalline
286 fractionation in tourmaline, with ^{10}B being preferentially incorporated at the T site relative to the
287 B site. Since the isotope fractionation is temperature-dependent, it is reasonable to assume a
288 temperature dependent effect of tetrahedral B on the value of $\Delta^{11}B_{tur\text{-}fluid}$. The influence of

289 temperature has not been investigated in this study but a first indication is provided by the results
290 of Kowalski et al. (2013). Based on the β factors presented therein, we deduced partial B isotope
291 fractionation between $^{[4]}B$ in tourmaline and fluid ($\Delta^{11}B_{[4]Btur\text{-}fluid}$) such as between $^{[3]}B$ and fluid
292 ($\Delta^{11}B_{[3]Btur\text{-}fluid}$), assuming only H_3BO_3 in the fluid, for temperatures between 350-700°C. With
293 these values the temperature-dependent intracrystalline B isotope fractionation for dravite and
294 olenite is calculated using equation (1).
295 The results suggest that the intracrystalline fractionation in olenite more than doubles from ~9‰
296 at 700°C to ~19‰ at 350°C (Fig. 5). For dravite the intracrystalline fractionation similarly
297 increases from ~7‰ at 700°C to ~16‰ at 350°C (Fig. 5). This is of particular importance,
298 because the incorporation of B at the T site is facilitated at lower temperatures (Ertl et al. 2008)
299 and hence the effect of $^{[4]}B$ on $\Delta^{11}B_{tur\text{-}fluid}$ is further enhanced.
300

301 ## IMPLICATIONS

302
303 It is shown that conventional $\Delta^{11}B_{tur\text{-}fluid}$ fractionation factors are not applicable to tourmalines
304 that incorporate excess B at the T site, which has consequences for the reconstruction of B
305 isotope signatures of coexisting aqueous fluids. If for example a tourmaline is considered that
306 crystallized at 700°C and has 22 mol% $^{[4]}B_{tot}$, which is the maximum amount observed in nature
307 (Ertl et al. 2008), the calculated $\delta^{11}B_{fluid}$ would be 0.7-2.9 ‰ more positive compared to the value
308 for $^{[4]}B$-free dravites using the fractionation factors of Meyer et al. (2008). Natural B isotope
309 variations in tourmaline from a given setting may commonly exceed this coordination-related
310 shift, but taking it into account reduces the overall uncertainty of using tourmaline isotope
311 signatures for geochemical modeling and fluid provenance studies (e.g. Bebout and Nakamura
312 2003; Berryman et al. 2017).

313 Since both the results of our study and those of Meyer et al. (2008) are in good agreement with
314 *ab initio* calculations of Kowalski et al. (2013), it is reasonable to assume that the latter are
315 accurate. This implies that for olenite with $^{[4]}B$ contents <10 mol% $^{[4]}B_{tot}$, the absolute value of
316 $\Delta^{11}B_{(tur\text{-}fluid)}$ is positive (Fig. 4) as opposed to negative for dravite, which is likely caused by the
317 shorter $^{[3]}B$-O bond length in olenite compared to dravite (Kowalski et al. 2013). This can be
318 important for the interpretation of B isotope patterns in natural tourmalines with compositions
319 close to olenite. Considering tourmaline growth in a closed system and at a small $[B]_{fluid}/[B]_{tur}$
320 ratio[3], $\Delta^{11}B_{(tur\text{-}fluid)} > 0$ would produce decreasing $\delta^{11}B_{tur}$ values in a core to rim profile, whereas
321 $\Delta^{11}B_{(tur\text{-}fluid)} < 0$ would produce increasing $\delta^{11}B_{tur}$ values.
322 This study also shows the importance of matrix-matched reference materials (RMs) for SIMS B
323 isotope analyses, which has implications for the analysis of tourmalines, which are strongly
324 compositionally zoned. If such tourmalines are measured from core to rim by SIMS using a
325 single RM, the $\delta^{11}B$ trends may be enhanced or depressed due to inappropriately matched RMs. It
326 must be said that many SIMS studies address the matrix effect by measuring multiple RMs and it
327 has commonly been considered to be negligible (e.g., Büttner and Kasemann 2007; Marschall et
328 al. 2006; Nakano and Nakamura, 2001). Our experience in the Potsdam SIMS laboratory shows
329 that the size of matrix effects can depend on the particular setup and instrument tuning and
330 cannot be ignored *a priori*.
331 Finally, intracrystalline B isotope fractionation in tourmaline potentially provides a
332 powerful tool to derive the pro- and retrograde temperature evolution using only a single
333 tourmaline crystal. This requires that $^{11}B/^{10}B$ ratios at the T and B sites in tourmaline are
334 measured separately, which is theoretically possible by calibrating the isotopic shift of vibrational
335 modes associated with $^{[3]}B/^{[4]}B$ based on vibrational spectroscopy. Hence the effect of

[3] [B] denotes the B concentration

336 temperature on the B isotope fractionation between $^{[4]}$B-bearing tourmaline and fluid needs to be
337 explored in greater detail and also as a function of tourmaline composition.
338
339 **ACKNOWLEDGMENTS**
340
341 F. Couffignal is acknowledged for his support during SIMS analyses. The authors thank U.
342 Dittmann for sample preparation, H.-P. Nabein for help with the XRD analysis and O. Appelt for
343 support during the EMP measurement. DFG founding granted to G. Franz (TU Berlin) and W.
344 Heinrich (GFZ Potsdam) (FR 557/31-1; HE 2015/16-1) is gratefully acknowledged. A. Meixner
345 acknowledges support from the DFG Major Research Instrumentation Program INST 144/308-1.
346 The quality of the manuscript benefitted a lot from the helpful comments of Horst Marschall and
347 Edward Grew.
348
349
350
351
352
353
354
355
356
357
358
359

REFERENCES

Armbruster, T., Buergi, H.B., Kunz, M., Gnos, E., Broennimann, S., and Lienert, C. (1990) Variations of displacement parameters in structure refinement of low albite. American Mineralogist, 75, 135-140.

Armstrong, J.T. (1995) CITZAF: a package of correlation programs for the quantitative electron microbeam X-ray analysis of thick polished materials, thin films, and particles. Microbeam Analysis, 4, 177-200.

Bebout, G.E., and Nakamura, E. (2003) Record in metamorphic tourmaline of subduction-zone devolatilization and boron cycling. Geology, 31, 407-410.

Berryman, E.J., Kutzschbach, M., Trumbull, R.B., Meixner, A., van Hinsberg, V., Kasemann, S.A., and Franz, G. (2017) Tourmaline as a petrogenetic indicator in Pfitsch Formation, Western Tauern Window, Eastern Alps. Lithos, in review.

Büttner, S.H., and Kasemann, S.A. (2007) Deformation controlled cation diffusion in tourmaline: a microanalytical study on trace elements and boron isotopes. American Mineralogist, 92, 1862-1874.

Catanzaro, E.J., Champion, C.E., Garner, E.L., Maienko, G., Sappenfield, K.M., and Shields,W.R. (1970) Boric Acid: Isotopic and assay standard reference materials. National Bureau of Standards (US) Special Publication 260-17, 70p.

Chaussidon, M., and Albarède, F. (1992) Secular boron isotope variations in the continental crust: an ion microprobe study. Earth and Planetary Science Letters, 108, 229-241.

Dyar, M.D., Wiedenbeck, M., Robertson, D., Cross, L.R., Delaney, J.S., Ferguson, K., Francis, C.A., Grew, E.S., Guidotti, C.V., Hervig, R.L., Hughes, J.M., Husler, J., Leeman, W., McGuire, A.V., Rhede, D., Rothe, H., Paul, R.L., Richards, I., and Yates, M. (2001) Reference minerals for the microanalysis of light elements. Geostandards Newsletter, 25, 441-463.

Ertl, A., Pertlik, F., and Bernhardt, H.-J. (1997) Investigations on olenite with excess boron from the Koralpe, Styria, Austria. Anzeiger Abt. I, 124, 3-10.

Ertl, A., Rossman, G.R., Hughes, J.M., Prowatke, S., and Ludwig, T. (2005) Mn-bearing „oxy-rossmanite" with tetrahedrally coordinated Al and B from Austria: Structure, chemistry, and infrared and optical spectroscopic study. American Mineralogist, 90, 481-487.

Ertl, A., Hughes, J.M., Prowatke, S., Ludwig, T., Prasad, P.S.R., Brandstätter, F., Körner, W., Schuster, R., Pertlik, F., and Marschall, H. (2006) Tetrahedrally coordinated boron in tourmaline from the liddicoatite-elbaite series from Madagascar: Structure, chemistry, and infrared spectroscopic studies. American Mineralogist, 91, 1847-1856.

Ertl, A., Hughes, J.M., Prowatke, S., Ludwig, T., Brandstätter, F., Körner, W., and Dyar, M.D. (2007) Tetrahedrally coordinated boron in Li-bearing olenite from „mushroom" tourmaline from Momeik, Myanmar. The Canadian Mineralogist, 45, 891-899.

Ertl, A., Tillmanns, E., Ntaflos, T., Francis, C., Giester, G., Körner, W., Hughes, J.M., Lengauer, C., and Prem, M. (2008) Tetrahedrally coordinated boron in Al-rich tourmaline and its relationship to the pressure-temperature conditions of formation. European Journal of Mineralogy, 20, 881-888.

Gonfiantini, R., Tonarini, S., Groening, M., Adorni-Braccesi, A., Al-Ammar, A., Astner, M., Baechler, S., Barnes, R.M., Bassett, R.L., Cocherie, A., Deyhle, A., Dini, A., Ferrara, G., Gaillardet, J., Grimm, J., Guerrot, C., Krahenbuehl, U., Layne, G., Lemarchand, D., Meixner, A., Northington, D.J., Pennisi, M., Reitznerova, E., Rodushkin, I., Sugiura, N.,

406 Surberg, R., Tonn, S., Wiedenbeck, M., Wunderli, S., Xiao, Y., and Zack, T. (2003)
407 Intercomparison of boron isotope and concentration measurements; part II, evaluation of
408 results. Geostandards Newsletter, 27, 41-57
409 Henry, D.J., and Dutrow, B.L. (1996) Metamorphic tourmaline and its petrological application.
410 Reviews in Mineralogy, 33, 503-557.
411 Hughes, J.M., Ertl, A., Dyar, M.D., Grew, E., Shearer, C.K., Yates, M.G., and Guidotti, C.V.
412 (2000) Tetrahedrally coordinated boron in a tourmaline: Boron-rich olenite from
413 Stoffhütte, Koralpe, Austria. The Canadian Mineralogist, 38, 861-868.
414 Hughes, J.M., Ertl, A., Dyar, M.D., Grew, E., Wiedenbeck, M., and Brandstätter F. (2004)
415 Structural and chemical response to varying $^{[4]}$B content in zoned Fe-bearing olenite from
416 Koralpe, Austria. The Canadian Mineralogist, 38, 447-454.
417 Kalt, A., Schreyer, W., Ludwig, T., Prowatke, S., Bernhardt, H.-J., and Ertl, A. (2001) Complete
418 solid solution between magnesian schorl and lithian excess-boron olenite in a pegmatite
419 from the Koralpe (eastern Alps, Austria). European Journal of Mineralogy, 13, 1191-1205.
420 Kasemann, S., Meixner, A., Rocholl, A., Vennemann, T., Rosner, M., Schmitt, A.K., and
421 Wiedenbeck, M. (2001) Boron and oxygen isotope composition of certified reference
422 materials NIST SRM 610/612 and reference materials JB-2 and JR-2. Geostandards
423 Newsletter, 25, 405-416.
424 Kihara, K. (1990) An X-Ray study of the temperature dependence of the quartz structure.
425 European Journal of Mineralogy, 2, 63-77.
426 Kowalski, P.M., and Wunder, B. (2017) Boron isotope fractionation among vapor-liquids-solids-
427 melts: experiments and atomistic modeling. In H.G. Marschall and G.L. Foster, Eds.,
428 Advances in Isotope Geochemistry – Boron Isotopes: The Fifth Element. Springer-Verlag,
429 Heidelberg, Berlin.
430 Kowalski, P.M., Wunder, B., and Jahn, S. (2013) Ab initio prediction of equilibrium boron
431 isotope fractionation between minerals and aqueous fluids at high *P* and *T*. Geochimica et
432 Cosmochimica Acta, 101, 285-301.
433 Krosse, S. (1995) Hochdrucksynthese, Stabilität und Eigenschaften der Borosilikate Dravit und
434 Kornerupin sowie Darstellung und Stabilitätsverhalten eines neuen Mg-Al-Borates.
435 Dissertation, Ruhr-Universität Bochum, Germany, 135 pp.
436 Kutzschbach, M., Wunder, B., Rhede, D., Koch-Müller, M., Ertl, A., Giester, G., Heinrich, W.,
437 and Franz, G. (2016) Tetrahedral boron in natural and synthetic HP/UHP tourmaline:
438 Evidence from Raman spectroscopy, EMPA, and single-crystal XRD. American
439 Mineralogist, 101, 93-104.
440 Kutzschbach, M., Wunder, B., Meixner, A., Wirth, R., Heinrich, W., and Franz, G. (2017)
441 Jeremejevite as a precursor for olenitic tourmaline: Consequences of non-classical
442 crystallization pathways for composition, textures and B isotope patterns of tourmaline in
443 synthesis experiments. European Journal of Mineralogy. (in press)
444 Larson, A.C., and Von Dreele, R.B. (1987) Generalized structure analysis system. Los Alamos
445 National Laboratory Report LA-UR-86-748.
446 MacGregor, J.R., Grew, E.S., De Hoog, J.C.M., Harley, S.L., Kowalski, P.M., Yates, M., and
447 Carson, C.J. (2013) Boron isotopic composition of tourmaline, prismatine, and
448 grandidierite from granulite facies paragneisses in the Larsemann Hills, Prydz Bay, East
449 Antartica: Evidence for a non-marine evaporite source. Geochimica et Cosmochimica
450 Acta, 123, 261-283.
451 Marschall, H.R., Ertl, A., Hughes, J.M., and McCammon, C. (2004) Metamorphic Na- and OH-
452 rich disordered dravite with tetrahedral boron associated with omphacite, from Syros,
453 Greece: chemistry and structure. European Journal of Mineralogy, 16, 817-823.

Marschall H.R., Ludwig, T., Altherr, R., Kalt, A., and Tonarini, S. (2006) Syros metasomatic tourmaline: Evidence for high-$\delta^{11}B$ fluids in subduction zones. Journal of Petrology, 47, 1915-1942.

Marschall, H., Meyer, C., Wunder, B., Ludwig, T., and Heinrich, W. (2009) Experimental boron isotope fractionation between tourmaline and fluid: confirmation from in situ analyses by secondary ion mass spectrometry and from Rayleigh fractionation modelling. Contributions to Mineralogy and Petrology, 158, 675-681.

Meyer, C., Wunder, B., Meixner, A., Romer, R.L., and Heinrich, W. (2008) Boron-isotopic fractionation between tourmaline and fluid: an experimental re-investigation. Contributions to Mineralogy and Petrology, 156, 259-267.

Nakano, T., and Nakamura, E. (2001) Boron isotope geochemistry of metasedimentary rocks and tourmalines in a subduction zone metamorphic suite. Physics of the Earth and Planetary Interiors, 127, 233-252.

Palmer, M.R., London, D., Morgan VI, G.B., and Babb, H.A. (1992) Experimental determination of fractionation of $^{11}B/^{10}B$ between tourmaline and aqueous vapor: A temperature- and pressure dependant isotopic system. Chemical Geology, 101, 123-129.

Romer R.L., Meixner A., and Hahne K. (2014) Lithium and boron isotopic composition of sedimentary rocks — The role of source history and depositional environment: A 250Ma record from the Cadomian orogeny to the Variscan orogeny. Gondwana Research, 26, 1093 - 1110.

Schmidt, C., Thomas, R., and Heinrich W. (2005) Boron speciation in aqueous fluids at 22 to 600°C and 0.1 MPa to 2GPa. Geochimica et Cosmochimica Acta, 69, 275-281.

Schreyer, W., Wodara, U., Marler, B., van Aken, P., Seifert, F., and Robert, J.-L. (2000) Synthetic tourmaline (olenite) with excess boron replacing silicon on the tetrahedral site: I. Synthesis conditions, chemical and spectroscopic evidence. European Journal of Mineralogy, 12, 529-541.

Schreyer, W., Hughes, J.M., Bernhardt, H-J., Kalt, A., Prowatke, S., and Ertl, A. (2002) Reexamination of olenite from the type locality: detection of boron in tetrahedral coordination. European Journal of Mineralogy, 14, 935-942.

Tagg, S.L., Cho, H., Dyar, M.D., and Grew, E.S. (1999) Tetrahedral boron in naturally occurring tourmaline. American Mineralogist, 84, 1451-1455.

Tonarini S., Pennisi M., and Leeman W.P. (1997) Precise boron isotopic analysis of complex silicate (rock) samples using alkali carbonate fusion and ion-exchange separation. Chemical Geology, 142, 129-137.

Tonarini, S., Pennisi, M., Adorni-Braccesi, A., Dini, A., Ferrara, G., Gonfiantini, R., Wiedenbeck, M., and Gröning, M. (2003) Intercomparison of boron isotope concentration measurements. Part I: Selection, preparation and homogeneity tests of the intercomparison materials. Geostandards Newsletter, 27, 21-39.

Van Hinsberg, V.J., Henry, D.J., and Marschall, H.R. (2011) Tourmaline: An ideal indicator of its host environment. The Canadian Mineralogist, 29, 1-16.

FIGURE CAPTIONS

Figure 1. Compositions of tourmaline reference materials in FeO-MgO-Al_2O_3 ternary space. Mean composition for dravite, schorl and elbaite from Dyar et al. (2001). Mean composition of B4 (fragment 3) is reported in Tonarini et al. (2003). The composition of the olenite RM is presented in this study (Table A1) and the data for synthetic olenites (red dot) is taken from Kutzschbach et al. (2016, 2017). The symbol size includes the uncertainty (1 SD).

Figure 2. Representative examples of synthetic olenites from the 216 h experiment used for *in situ* B isotope analysis by SIMS. BSE images were acquired after SIMS analysis. a) columnar olenite with jeremejevite and coesite inclusions b) inclusion-free columnar olenite c) acicular olenite. All crystals are cut in orientation ± parallel to the *c*-axis. The white circle marks the analysis spot. Analysis of the rim of the acicular crystal has been neglected as the SIMS spot hit a crack. White particles are remnants of the gold coating.

Figure 3. B isotope ratios of synthetic olenites from the 216 h experiment determined by SIMS. $\delta^{11}B$ values are obtained in session S1 and S2 by IMF correction using a particular tourmaline reference material. Additionally, $\delta^{11}B$ values of the initial fluid and quenched fluids extracted after 0.5 h and 216 h run as reported in Kutzschbach et al. (2017) are presented (grey bars). Note that the difference in B isotope ratios for a given RM is significant between any two crystal populations. Similarly a significant difference in B isotope ratios is observed for a given crystal population using different RM.

525 **Figure 4.** Variation of B isotope fractionation between tourmaline and fluid ($\Delta^{11}B_{tur\text{-}fluid}$) with
526 $^{[4]}B_{tot}$ in tourmaline. Colored squares illustrate $\Delta^{11}B_{tur\text{-}fluid}$ obtained in this study by calculating
527 $\delta^{11}B_{tur}$-$\delta^{11}B_{fluid}$ using synthetic olenitic tourmaline and various tourmaline reference materials for
528 IMF correction (Table 3). The white square indicates the results obtained from Rayleigh
529 fractionation modeling of the B isotope evolution of the fluid (see text). Solid lines indicate the
530 $\Delta^{11}B_{tur\text{-}fluid}$ for olenite (black) and dravite (grey) at 0.1MPa based on *ab initio* calculations by
531 Kowalski et al. (2013) assuming only trigonal H_3BO_3 in the fluid. The dashed line shows $\Delta^{11}B_{tur\text{-}}$
532 $_{fluid}$ for olenite assuming 15 mol% $(H_4BO_4)^-$ in the fluid. Uncertainty on the prediction of
533 Kowalski et al. (2013) is indicated by the grey shaded area and are similar for all datasets. A star
534 indicates $\Delta^{11}B_{tur\text{-}fluid}$ at 0.2 GPa experimentally determined for dravite by Meyer et al. (2008). All
535 data for T = 700°C.

536

537 **Figure 5.** Intracrystalline fractionation between trigonal B ($^{[3]}B$) and tetrahedral B ($^{[4]}B$) in
538 dravite and olenite based on β factors presented in Kowalski et al. (2013). The dotted lines are
539 guide to the eye.

540

541 **Figure A1**. Backscattered electron image of the olenite reference material used for SIMS and
542 EMP analyses. Tourmaline (tur) shows slight patchy zonation with BSE light and BSE dark areas
543 and is intimately intergrown with quartz (qtz), albite (ab), and muscovite (ms).

544
545
546
547
548
549
550
551
552
553

Figure 1

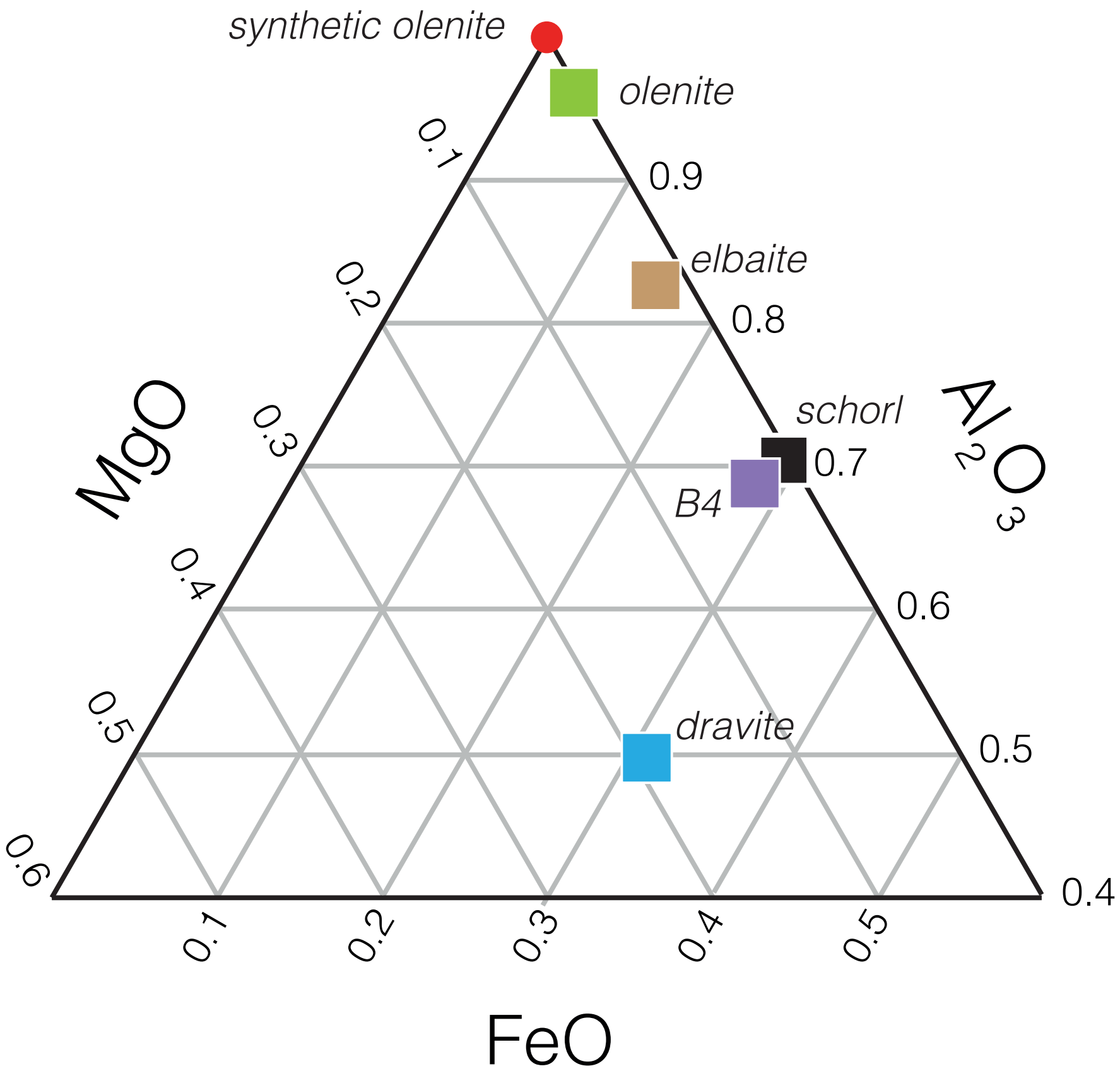
synthetic olenite
olenite
elbaite
schorl
B4
dravite
MgO
Al2O3
FeO
0.1
0.2
0.3
0.4
0.5
0.6
0.9
0.8
0.7
0.6
0.5
0.4
0.6
0.5
0.4
0.3
0.2
0.1

Figure 2

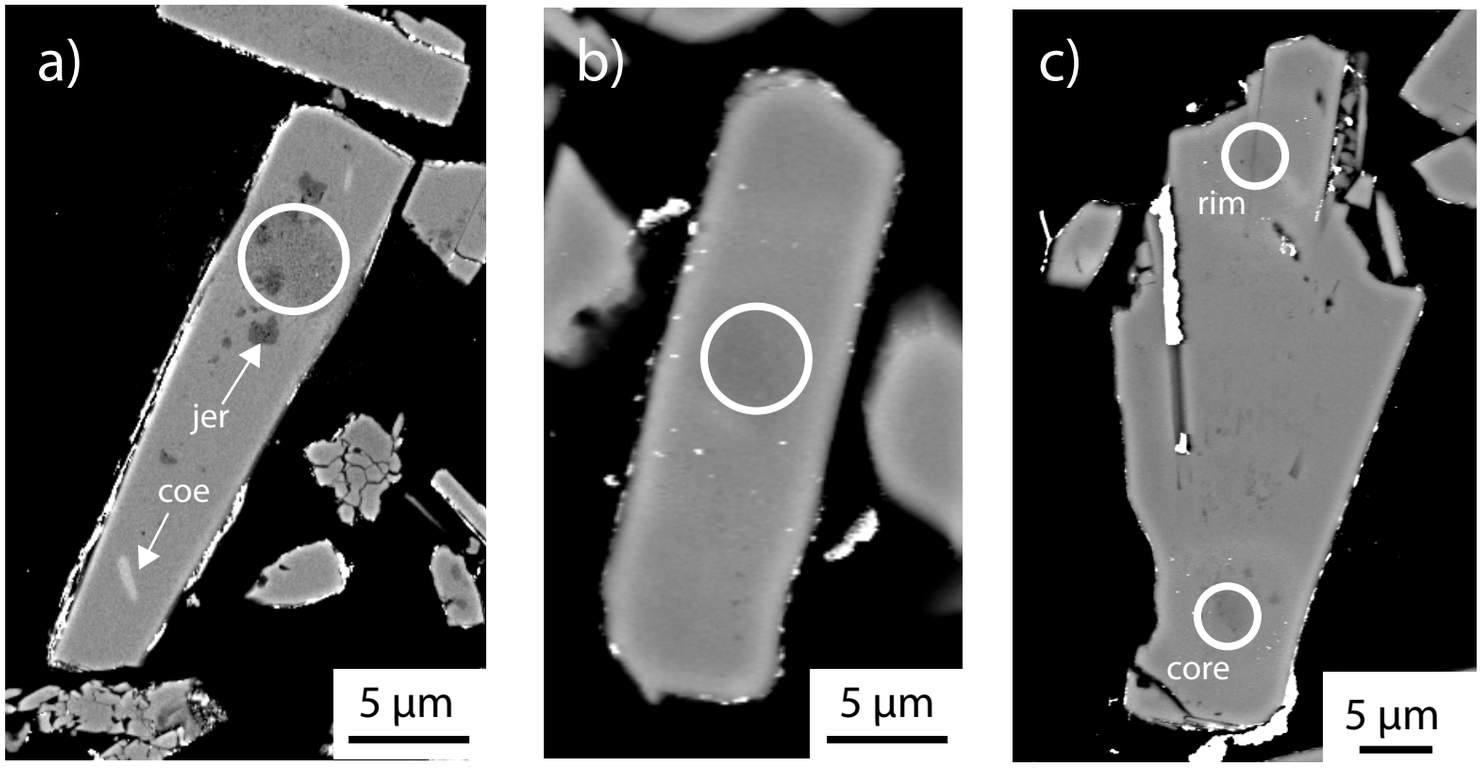

Figure 3

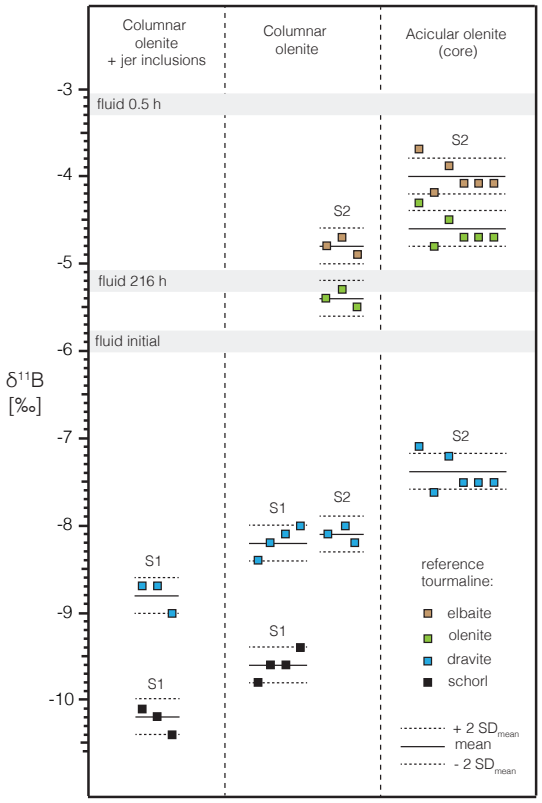
Columnar olenite + jer inclusions
Columnar olenite
Acicular olenite (core)
fluid 0.5 h
fluid 216 h
fluid initial
δ11B [‰]
-3
-4
-5
-6
-7
-8
-9
-10
S1
S2
reference tourmaline:
elbaite
olenite
dravite
schorl
+ 2 SDmean
mean
- 2 SDmean

Figure 4

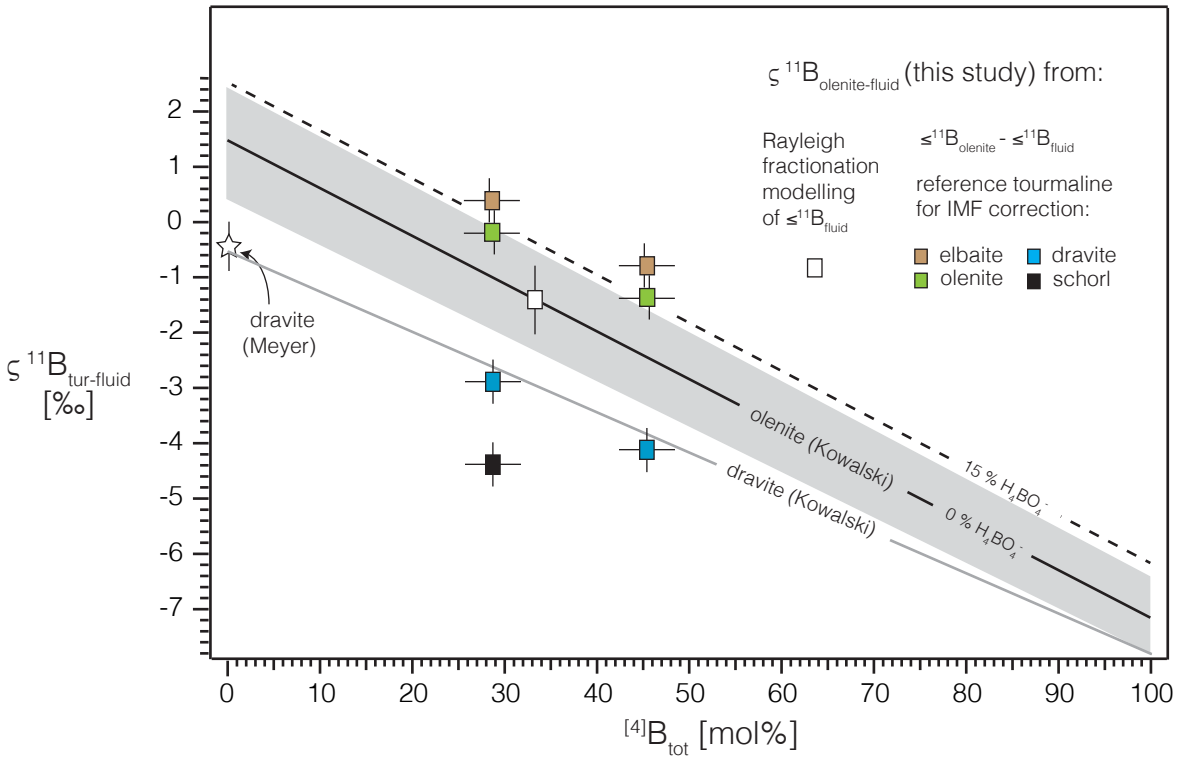
ς 11Bolenite-fluid (this study) from:
Rayleigh fractionation modelling of ≤11Bfluid
≤11Bolenite - ≤11Bfluid
reference tourmaline for IMF correction:
elbaite
dravite
olenite
schorl
dravite (Meyer)
olenite (Kowalski)
dravite (Kowalski)
15 % H3BO3
0 % H3BO3
ς 11Btur-fluid [‰]
[4]Btot [mol%]
2
1
0
-1
-2
-3
-4
-5
-6
-7
0
10
20
30
40
50
60
70
80
90
100

Figure 5

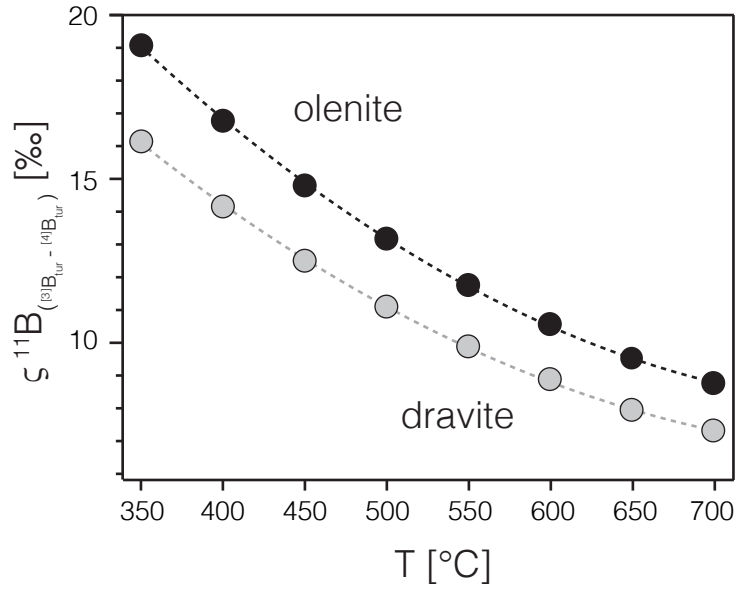
20
15
10
olenite
dravite
350
400
450
500
550
600
650
700
T [°C]
ε 11B([3]Btur - [4]Btur) [‰]

Table 1. B isotope ratios and B concentration of quenched experimental fluids

run duration	**0.5 h**	**216 h**
$\delta^{11}B_{fluid\ fin}$ [‰]	-3.2 (2)	-5.2 (2)
$B_{fluid\ fin}$ [a] [µg/g]	8.9 (5)	13.8 (8)
$B_{fluid\ fin}$ [b] [mg]	0.45	0.69
$B_{fluid\ ini}$ [c] [mg]	1.19	1.16
F [d]	0.38	0.60

Errors are based on the external reproducibility and are indicated in brackets. Starting boric acid ($\delta^{11}B_{fluid\ ini}$) has a value of -5.9(1) ‰. Data taken from Kutzschbach et al. (2017).

[a] B concentration in the final fluid determined by MC-ICP-MS

[b] weight of B in the final fluid calculated from $B_{fluid\ fin}$ [µg/g], the volume of diluted fluid (50 ml) and $\rho(H_2O)$ =1 g/ml

[c] weight of B in the initial fluid calculated from weight of H_3BO_3 in the starting material

[d] F is the fraction of B remaining in the fluid. F = $B_{fluid\ fin}$ [mg]/ $B_{fluid\ ini}$ [mg]

Table 2. Summary of SIMS B isotope analyses of tourmaline reference materials

analysis date	n	$(^{11}B/^{10}B)_{meas}$	2 RSD_{mean} [‰][a]	IMF[b]	$\delta^{11}B$ [‰][c]
schorl 112566: $(^{11}B/^{10}B)_{real}$ = 3.993 and $\delta\ ^{11}B$ = -12.5					
07/28/2015 (S1)	3	3.896	0.20	0.9757	-11.7
2 RSD [‰][d]		0.28		0.28	
dravite 108796: $(^{11}B/^{10}B)_{real}$ = 4.017 and $\delta\ ^{11}B$ = -6.6					
07/28/2015 (S1)	3	3.913	0.34	0.9741	-7.4
2 RSD [‰][d]		0.62		0.62	
06/06/2016 (S2)	5	3.930	0.22	0.9783	-4.5
2 RSD [‰][d]		0.36		0.36	
elbaite 98114: $(^{11}B/^{10}B)_{real}$ = 4.001 and $\delta\ ^{11}B$ = -10.5					
06/06/2016 (S2)	16	3.901	0.26	0.9750	-11.9
2 RSD [‰][d]		0.62		0.62	
olenite Koralpe: $(^{11}B/^{10}B)_{real}$ = 4.038 and $\delta\ ^{11}B$ = -1.4					
06/06/2016 (S2)	13	3.940	0.30	0.9757	-2.0
2 RSD [‰][d]		0.96		0.96	

Note: $(^{11}B/^{10}B)_{meas}$, internal precision, IMF and $\delta^{11}B$ given as daily average of each tourmaline RM

[a] internal precision for a single analysis consisting of 20 cycles
RSD_{mean} (‰) = [(standard deviation/√20)/mean]*1000.

[b] Instrumental mass fractionation; IMF = $(^{11}B/^{10}B)_{meas}$/ $(^{11}B/^{10}B)_{real}$
$(^{11}B/^{10}B)_{real}$ for schorl, dravite, elbaite from Dyar et al. (2001)
$(^{11}B/^{10}B)_{real}$ for olenite see appendix in this study

[c] Corrected with daily average IMF of all reference tourmalines with 0.9749 (07/28/2015 = S1) and 0.9763 (06/06/2016 = S2) and calculated relative to $^{11}B/^{10}B$ = 4.04362 of NBS SRM 951

[d] repeatability based on multiple analyses of each tourmaline RM
RSD (‰) = (standard deviation / mean) * 1000.

Table 3. $\delta^{11}B_{tur}$ values of synthetic olenites from the 216 h experiment

session	n	$\delta^{11}B_{tur}$ [‰][a] RM used for IMF correction			
		olenite	*elbaite*	*dravite*	*schorl*
columnar					
S1	4	/	/	-8.2(2)	-9.6(2)
S2	3	-5.4(2)	-4.8(2)	-8.1(2)	/
columnar + jeremejevite inclusions					
S2	3	/	/	-8.8 (2)	-10.2 (2)
acicular					
S2	6	-4.6(2)	-4.0(2)	-7.4(2)	/

[a] Corrected with daily average IMF of a particular RM (see Table 2) and calculated relative to $^{11}B/^{10}B = 4.04362$ of NBS SRM 951

Numbers in brackets denote the standard deviation from the mean (2 SD_{mean}).

$SD_{mean} = SD/\sqrt{n}$

Table 4. Stable B isotope fractionation between tourmaline and fluid at 4.0 GPa/700°C

$^{[4]}B_{tot}$ [mol%] in tourmaline	Crystal	$\Delta^{11}B_{(tur\text{-}fluid)}$ [‰] RM used for IMF correction			
		olenite	*elbaite*	*dravite*	*schorl*
29(3)	columnar	-0.2 ± 0.4	0.4 ± 0.4	-2.9 ± 0.4	-4.4 ± 0.4
45(3)	acicular (core)	-1.4 ± 0.4	-0.8 ± 0.4	-4.1 ± 0.4	

$\Delta^{11}B_{(tur\text{-}fluid)}$ calculated with $\delta^{11}B_{tur} - \delta^{11}B_{fluid}$. Uncertainty of $\Delta^{11}B_{(tur\text{-}fluid)}$ is estimated by adding the uncertainty of $\delta^{11}B_{tur}$ (Table 3) and the uncertainty of $\delta^{11}B_{fluid}$ (Table 1). $^{[4]}B_{tot}$ of columnar olenites and cores of the acicular olenites from Kutzschbach et al. (2016). For more information see text.